Geophysical Research Letters

RESEARCH LETTER
10.1029/2020GL087944

Uncertainties of Glacial Isostatic Adjustment Model Predictions in North America Associated With 3D Structure

Tanghua Li[1], Patrick Wu[2,3], Hansheng Wang[4], Holger Steffen[5], Nicole S. Khan[2], Simon E. Engelhart[6], Matteo Vacchi[7], Timothy A. Shaw[8], W. Richard Peltier[9], and Benjamin P. Horton[1,8]

[1]Earth Observatory of Singapore, Nanyang Technological University, Singapore, Singapore, [2]Department of Earth Sciences and the Swire Marine Institute, University of Hong Kong, Hong Kong, [3]Department of Geoscience, University of Calgary, Calgary, Alberta, Canada, [4]State Key Laboratory of Geodesy and Earth's Dynamics Institute of Geodesy and Geophysics, Chinese Academy of Science, Wuhan, China, [5]Geodata Division, Lantmäteriet, Gävle, Sweden, [6]Department of Geography, Durham University, Durham, UK, [7]Dipartimento di Scienze della Terra, Università di Pisa, Pisa, Italy, [8]Asian School of the Environment, Nanyang Technological University, Singapore, Singapore, [9]Department of Physics, University of Toronto, Toronto, Ontario, Canada

Abstract We quantify GIA prediction uncertainties of 250 1D and 3D glacial isostatic adjustment (GIA) models through comparisons with deglacial relative sea-level (RSL) data from North America and rate of vertical land motion ($\dot{U}$) and gravity rate of change ($\dot{G}$) from GNSS and GRACE data, respectively. Spatially, the size of the RSL uncertainties varies across North America with the largest from Hudson Bay and near previous ice margins along the northern Atlantic and Pacific coasts, which suggests 3D viscosity structure in the lower mantle and laterally varying lithospheric thickness. Temporally, RSL uncertainties decrease from the Last Glacial Maximum to present except for west of Hudson Bay and the northeastern Pacific coast. The uncertainties of both these regions increase from 30 to 45 m between 15 and 11 ka BP, which may be due to the rapid decrease of surface loading at that time. Present-day $\dot{U}$ and $\dot{G}$ uncertainties are largest in southwestern Hudson Bay with magnitudes of 2.4 mm/year and 0.4 μGal/year, mainly due to the 3D viscosity structure in the lower mantle.

Key Points:
- We predict the GIA signal with uncertainties of RSL and present-day $\dot{U}$ and $\dot{G}$ in North America that are associated with 3D structures
- GIA-predicted RSL uncertainties are largest around Hudson Bay and near former ice margins along northern Atlantic and Pacific coasts
- The maximum uncertainties of present-day $\dot{U}$ and $\dot{G}$ are centered in southwestern Hudson Bay and near former ice margins

Supporting Information:
- Supporting Information S1

Correspondence to:
T. Li,
li.tanghua@ntu.edu.sg;
li.tanghua@connect.hku.hk

Citation:
Li, T., Wu, P., Wang, H., Steffen, H., Khan, N. S., Engelhart, S. E., et al. (2020). Uncertainties of glacial isostatic adjustment model predictions in North America associated with 3D structure. *Geophysical Research Letters*, *47*, e2020GL087944. https://doi.org/10.1029/2020GL087944

Received 12 MAR 2020
Accepted 5 APR 2020
Accepted article online 17 APR 2020

1. Introduction

Glacial isostatic adjustment (GIA) studies are vital to interpret relative sea-level (RSL) change, present-day rates of vertical land motion ($\dot{U}$), and gravity-rate-of-change ($\dot{G}$) signals with respect to the growth and decay of Quaternary ice sheets (e.g., Peltier, 2005; Schumacher et al., 2018). Due to the imperfect knowledge of GIA model inputs (i.e., models of the surface loading history and Earth's internal viscoelastic structure), it is desirable to quantify the uncertainties of GIA predictions from an ensemble of GIA models (Caron et al., 2018; Melini & Spada, 2019). GIA uncertainties have previously been derived from (1) 20% of the magnitudes of the signal of interest (e.g., Karegar et al., 2017; Slangen et al., 2012) for time-dependent gravity measurements of the Gravity Recovery And Climate Experiment (GRACE) twin-satellite mission, (2) using (semi)empirical estimation (e.g., Hill et al., 2010; Riva et al., 2009; Simon et al., 2017), and (3) residual misfit analysis (e.g., Peltier et al., 2015).

Recent advances in computational power have enabled GIA uncertainties to be estimated using a large ensemble of randomly generated ice-Earth models (e.g., Caron et al., 2018; Melini & Spada, 2019). However, the Earth component of GIA models has used 1D (laterally homogeneous) viscosity models that neglect the influence of 3D structure. Surface geology (e.g., Kennett & TkalČić, 2008) and seismic tomography (e.g., Bunge & Grand, 2000) show that Earth's material properties are laterally heterogeneous and many studies have revealed that the 3D structure has a significant influence on GIA predictions (e.g., Austermann et al., 2013; Li et al., 2018; Yousefi et al., 2018). Indeed, 3D structure has been invoked as a mechanism whereby GIA models may better fit late Quaternary RSL records (e.g., Clark et al., 2019; Kuchar et al., 2019; Love et al., 2016), while neglecting 3D structure could introduce bias in 1D viscosity inversions (Lau et al., 2018).

The GIA prediction uncertainties of RSL, $\dot{U}$, and $\dot{G}$ can be separated into two types (Melini & Spada, 2019): (1) uncertainties associated with input parameters of the Earth rheology model or surface mass loading history of continental ice sheets (T1) and (2) uncertainties associated with structural differences among GIA models that use different methods to solve the sea-level equation, such as the implementation or neglect of coastline migration (T2). Here, we subdivide the T1 uncertainties into those associated with Earth model only (T1A), with surface loading history only (T1B) and with both Earth model and surface loading history (T1C) (see Text S1 in the supporting information for detailed discussion on GIA uncertainties and the strategy of this paper). In this paper, we use the surface loading history of ICE-6G_C (Argus et al., 2014; Peltier et al., 2015) and restrict our analysis to North America, where quality-controlled RSL data are densely distributed along the coasts and previous analysis has revealed misfits between 1D GIA models and the data (e.g., Roy & Peltier, 2015). Our goal is to isolate the T1A GIA prediction uncertainties for an ensemble of Earth models. The ensemble has 250 Earth models in total, including 150 3D Earth models. The 3D structure contains lateral variations in mantle viscosity, lithospheric thickness, and sublithospheric and asthenospheric properties (Figure S1).

To calculate the T1A uncertainties, we select a subset of GIA models from the large ensemble based on the ability of model predictions to fit simultaneously: (1) the latest quality-controlled deglacial RSL databases from the Atlantic (Engelhart & Horton, 2012; Vacchi et al., 2018) and Pacific coasts of North America (Engelhart et al., 2015) and (2) observed present-day $\dot{U}$ and $\dot{G}$ data in North America from Global Navigation Satellite System (GNSS) and GRACE data. Present-day horizontal motion data are not considered here because they have not been used to constrain the ICE-6G_C model (Peltier et al., 2015). We investigate the GIA prediction uncertainties using 3D global structure, thereby laying the groundwork for future studies that also consider uncertainty in surface loading history (e.g., T1C) and the separation of uncertainties due to surface loading history and Earth model parameters.

2. Methods

The GIA response of a spherical, self-gravitating, materially compressible Maxwell Earth is computed using the Coupled Laplace-Finite Element method (Wu, 2004). The effects of rotational feedback and time-dependent coastlines are also included in the computation of the solution to the sea-level equation (Clark et al., 1978). Our finite element grid has a 0.5× 0.5° spatial resolution near the surface but decreases with depth to 2.0× 2.0° in the lower mantle to reduce computation time. Note that when the Coupled Laplace-Finite Element method is employed to reconstruct the results for the ICE-6G_C (VM5a) model of Peltier et al. (2015) that was computed with conventional spectral-normal mode method, Text S2 and Figure S2 show that RSL and present-day $\dot{U}$ predictions are very closely recovered.

We search the parameter space of models with varying (1) laterally heterogeneous mantle viscosity, (2) lateral thickness of an elastic lithosphere, and (3) viscosity and lateral thickness of the sublithosphere and asthenosphere that can fit deglacial RSL data and the observed present-day $\dot{U}$ and $\dot{G}$ measurements in North America simultaneously (Li et al., 2018; Li & Wu, 2018) (see Texts S3 and S4 and Table S1 for further details concerning the search algorithm). The lateral viscosity variations in the mantle are derived from shear wave velocity anomalies in a global seismic tomography model (Karato, 2008; Wu et al., 2013). We employ the Bunge and Grand's (2000) seismic tomography model with scaling factors to search for 3D viscosity model solutions. We note that use of a different seismic tomography model, S20A of Ekström and Dziewonski (1998), does not significantly affect which combination of parameters and scaling factors produces the best-fitting model (Li et al., 2018). The lateral variation of lithospheric thickness is, however, derived from model S20A (Ekström & Dziewonski, 1998). The importance of lateral thickness variations in the lithosphere (or lack thereof) has been discussed by Nield et al. (2018), Spada et al. (2006), Wu et al. (2010), and others.

We compare GIA predictions to a quality-controlled deglacial RSL database from the Atlantic (Engelhart & Horton, 2012; Vacchi et al., 2018) and Pacific coasts of North America (Engelhart et al., 2015), which is also updated with relevant new published reconstructions (e.g., Hawkes et al., 2016; Khan et al., 2017; Love et al., 2016; Figure S3, Text S4). This combined data set contains 3,368 data points in total, including 1,725 sea-level index points, which define the elevation of RSL at a given point in space and time, and 874 marine limiting and 769 terrestrial limiting data points, which provide lower and upper limits on the

position of RSL (Figure S3), respectively (Engelhart & Horton, 2012; Shennan & Horton, 2002). We selected 24 regions from the Atlantic and Pacific coasts of North America, prioritizing RSL records that are temporally complete across during the Holocene (12,000 years to present, Figure 2a).

We compare present-day $\dot{U}$ and $\dot{G}$ predictions from the ensemble of GIA models with observations processed from GNSS (Figure 3a) and GRACE data that were used to constrain (GPS observations) and/or validate (GRACE observations) the ICE-6G_C model in Peltier et al. (2015). Additionally, we use the GIA induced $\dot{G}$ signal transformed from GNSS data (see Wang et al. (2013) for methodology, Figure S4) for comparison with the present-day $\dot{G}$ predictions (Figure 3c).

We calculate the misfit χ statistics between deglacial RSL data, observed present-day $\dot{U}$ and $\dot{G}$ data and the values predicted from 250 GIA models (including 150 3D GIA models) to select the subset of GIA models for uncertainty calculation (Text S4). Among the subset of GIA models, the mean and standard deviation of model predictions of RSL, $\dot{U}$, and $\dot{G}$ are calculated as follows:

$$\overline{p_i} = \frac{1}{N}\sum_{j=1}^{N} p_i(m_j), \tag{1}$$

$$\sigma_i = \sqrt{\frac{1}{N}\sum_{j=1}^{N}\left(p_i(m_j) - \overline{p_i}\right)^2}, \tag{2}$$

where N represents the number of best-fitting model selected, $p_i(m_j)$ indicates the ith prediction (e.g., at time t_i at a given RSL site) of model m_j, $\overline{p_i}$ represents the mean of the ith prediction, and σ_i represents the standard deviation of the ith prediction. Here, we take $2\sigma_i$ as the ith prediction uncertainty. Note that our statistics (equations 1 and 2) are different from those previously employed (e.g., Melini & Spada, 2019) and, therefore, the results are not directly comparable.

3. Results and Discussion

Based on the goodness of fit with the deglacial RSL data and the observed present-day $\dot{U}$ and $\dot{G}$ data in North America, we select the 10 best-fitting models (Text S4 and Table S2) from 250 GIA models (including 150 3D GIA models) to compute the mean and 2σ uncertainties of GIA predictions of RSL, $\dot{U}$, and $\dot{G}$. A subset of 5 or 20 best-fitting models does not significantly alter the mean and 2σ uncertainties (Text S4, Figures 1, 3, and S5–S8). The uncertainties of 10 best-fitting models encompass a reasonable range of GIA predictions of RSL, $\dot{U}$, and $\dot{G}$ with different 3D parameters in the Earth model. The 10 best-fitting models include five 3D models, two 1D models, and three models with 1D mantle viscosity but laterally varying lithosphere, sublithosphere and asthenosphere (Text S4 and Table S2).

3.1. Deglacial RSL Uncertainties

The mean of the 10 best-fitting GIA models shows two maxima of RSL in western and eastern Hudson Bay which decrease from the Last Glacial Maximum to present: >600 m at 15 ka BP, >300 m at 9 ka BP, and > 120 m at 6 ka BP (Figure 1). During deglaciation, mean RSL gradually migrates northeastwards from the west of Hudson Bay between 15 and 9 ka BP. This pattern is mainly due to the melting of two ice domes in western and eastern Hudson Bay in ICE-6G_C (Peltier et al., 2015).

The 2σ uncertainties of the RSL predictions show a different pattern to the mean (Figures 1 and S5) with larger uncertainties west and east of Hudson Bay (~ 30 m at 15 ka BP) and near previous ice margins of the Laurentide ice sheet along the northern Atlantic and Pacific coasts (~20 m at 15 ka BP). Temporally, the magnitude of RSL 2σ uncertainties decreases from Last Glacial Maximum to present in most locations. However, there is an increase in the magnitude of the RSL 2σ uncertainties from 30 to 45 m between 15 and 11 ka BP (Figure S5) west of Hudson Bay and the north Pacific coast, which is related to the fast release of surface loading (Figure S9) from the Meltwater Pulses 1A and 1B (Fairbanks, 1989) in the ICE-6G_C reconstruction that are primarily sourced from the Laurentide ice sheet (Peltier et al., 2015). Spatially, the patterns of RSL 2σ uncertainties are similar from 15 to 8 ka BP, after which areas of higher uncertainties (15 m at 7 ka BP and ≥1 m at 1 ka BP in Figure S5) emerge from southwest Hudson Bay to southern Saskatchewan and along northern Atlantic and Pacific coasts of

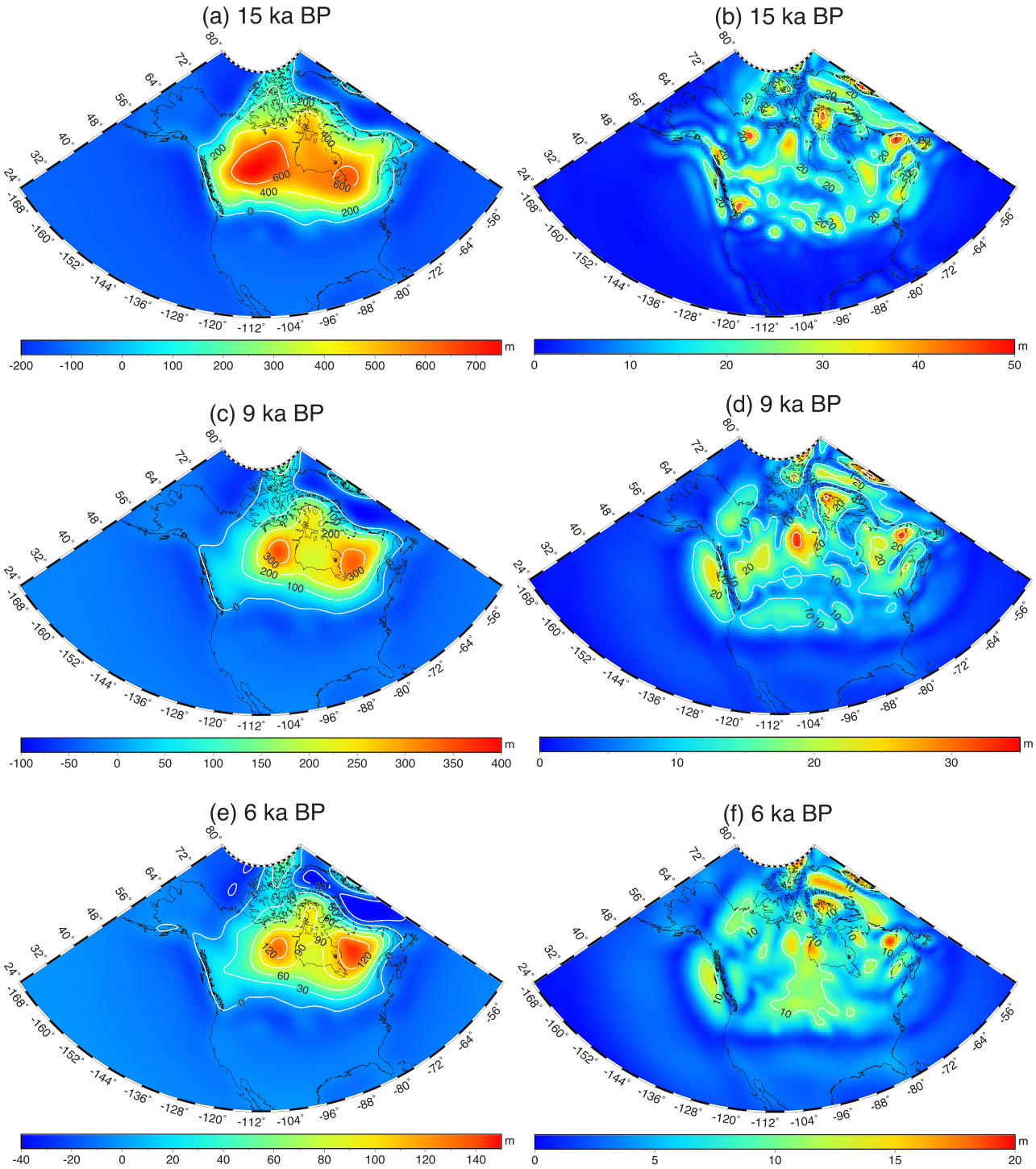

Figure 1. The mean relative sea-level (RSL) (left panel) and 2σ uncertainties of RSL (right panel) in North America. The 2σ uncertainties of RSL at 26 ka BP and 18–1 ka BP at 1 ka interval are shown in Figure S5.

North America. Because all ice has melted from North America by ~8 ka BP (Peltier et al., 2015), we suggest these uncertainties may be entirely due to the uncertainties in the 3D viscosity structures in the mantle. Indeed, Love et al. (2016) and Yousefi et al. (2018) concluded that northern Atlantic and Pacific coasts are sensitive to 3D structure.

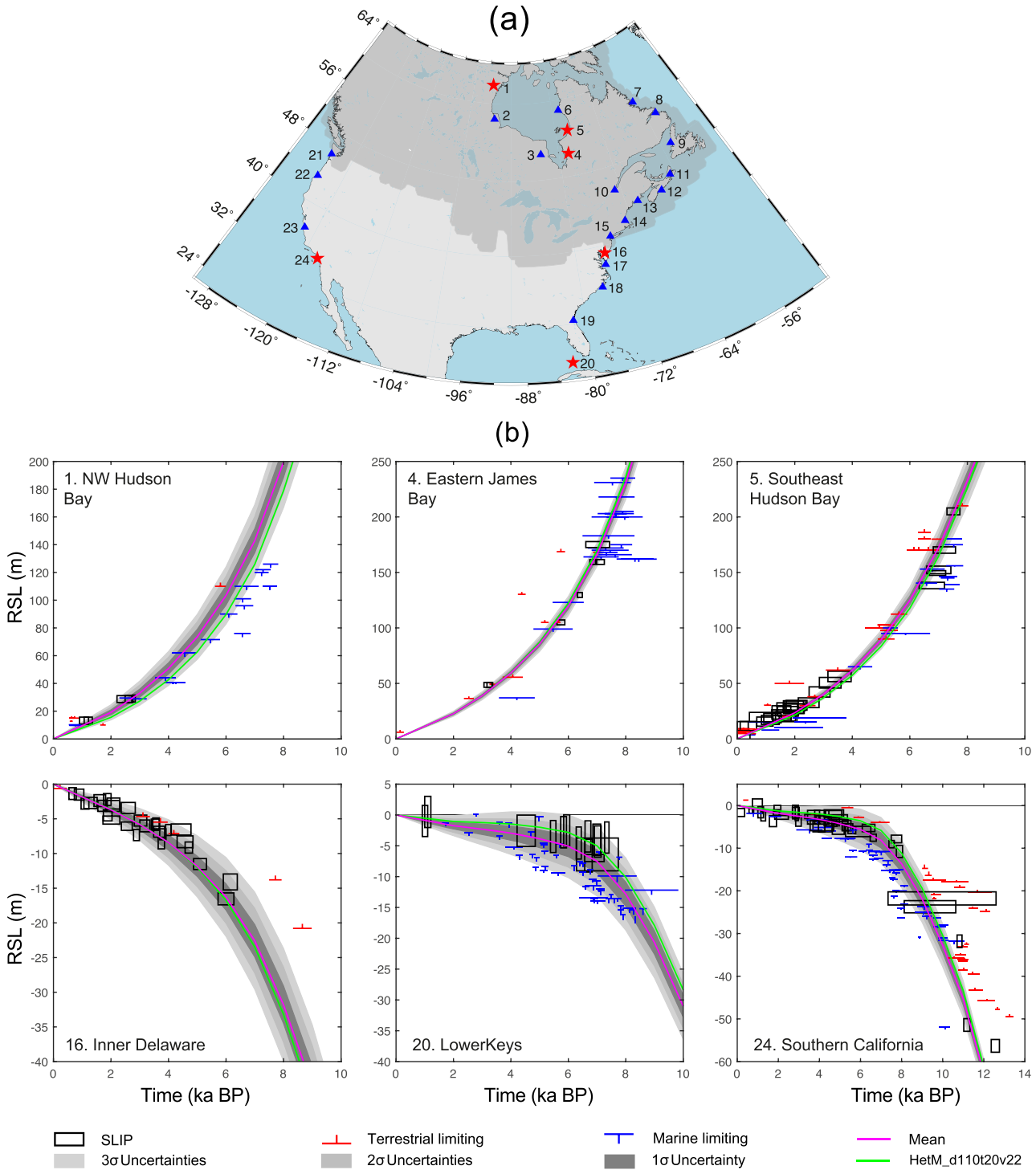

Figure 2. Locations of the 24 deglacial relative sea-level (RSL) study sites (red stars and blue triangles in a). The gray-shaded area in (a) represents the ice coverage at LGM (26 k BP) of ICE-6G_C. RSL curves at six sites (red stars in a) predicted by different models (see text) compared with deglacial RSL data from the combined data set (b). SLIPs are plotted as boxes with 2σ vertical and calibrated age errors. The marine limiting provides a lower constraint and the terrestrial limiting provides an upper constraint on RSL. The purple solid line represents the mean RSL; the green solid line represents the best-fitting 3D model (HetM-D110t20v22) in North America. The dark gray-, gray-, and light gray-shaded areas indicate the 1σ, 2σ, and 3σ uncertainties from the mean RSL, respectively. The complete 24 sites RSL curves are shown in Figure S10.

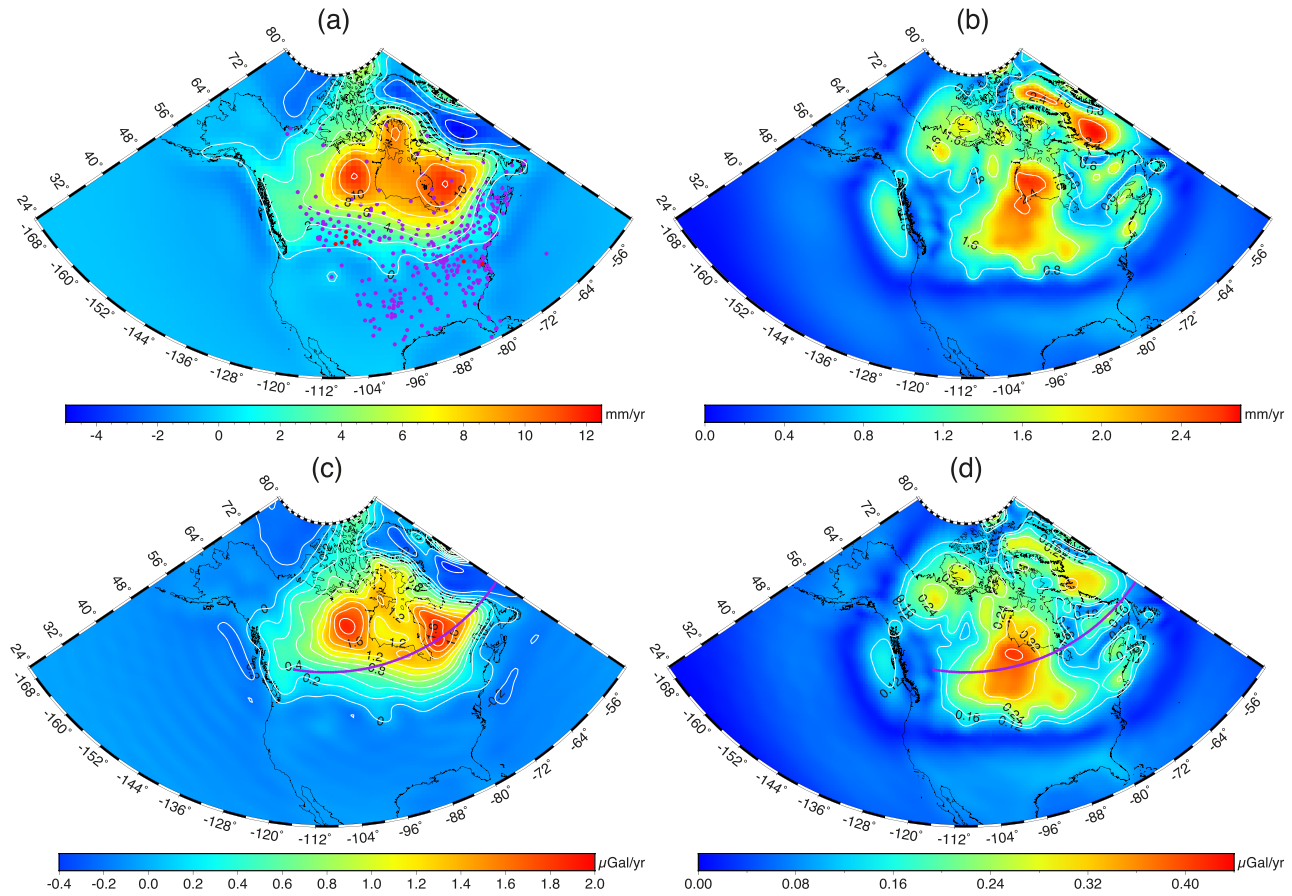

Figure 3. Mean present-day (a) $\dot{U}$ and (c) $\dot{G}$ and their corresponding 2σ uncertainties in (b) and (d), respectively. The purple dots and red dots in (a) represent GNSS stations from Peltier et al. (2015). The former indicates that our mean present-day $\dot{U}$ with 2σ uncertainties fits with the observed GNSS data at that site, while the latter fits within two times the errorbars. The purple lines (c and d) represent the 54°N cross section shown in Figure 4.

We compared the mean RSL predictions of the 10 best-fitting models and the RSL predictions of the best-fitting model HetM-d110t20v22 (Text S4 and Table S2) with the deglacial RSL data from the 24 selected regions (Figures 2 and S10). The best-fitting model HetM-d110t20v22 includes 3D viscosity structure in the mantle but a lithosphere of uniform thickness—this is because we searched the parameter space of the 3D viscosity structures with a uniformly thick lithosphere (Li et al., 2018). Of the 250 models considered, the model that least fit the data is a 3D model with VM5a as 1D background viscosity model and scaling factors equal 1 (Figure S11).

The mean RSL with 3σ uncertainties and the predictions of model HetM-d110t20v22 fit most of the deglacial RSL data from near (e.g., regions 1–6 and 11–13) and intermediate (e.g., regions 15–17, 20–21, and 24) study regions (Figures 2b and S10), which validates the performance of our selected models. The RSL uncertainties are relatively small in the near field around Hudson Bay and James Bay (e.g., regions 3–6) compared to the large RSL magnitudes in these regions (e.g., >180 m at 8 ka BP for regions 3–6). RSL uncertainties are also small in the intermediate field distant from the Laurentide ice sheet margins (e.g., regions 17–18 and 22–24, Figures 2b and S10).

The largest RSL uncertainties are found in regions close to the ice margins (e.g. regions 7–9 and 13–15, Figure S10). The locations of these large uncertainties may be related to forebulge migration toward the ice center as the regions experienced both GIA-related uplift early in deglaciation but forebulge collapse later (e.g., Barnhardt et al., 1995; Roy & Peltier, 2015; Stea et al., 2001; Tushingham & Peltier, 1991). Wang and Wu (2006) suggested that forebulge areas (e.g., regions 13–15) are sensitive to the 3D Earth models.

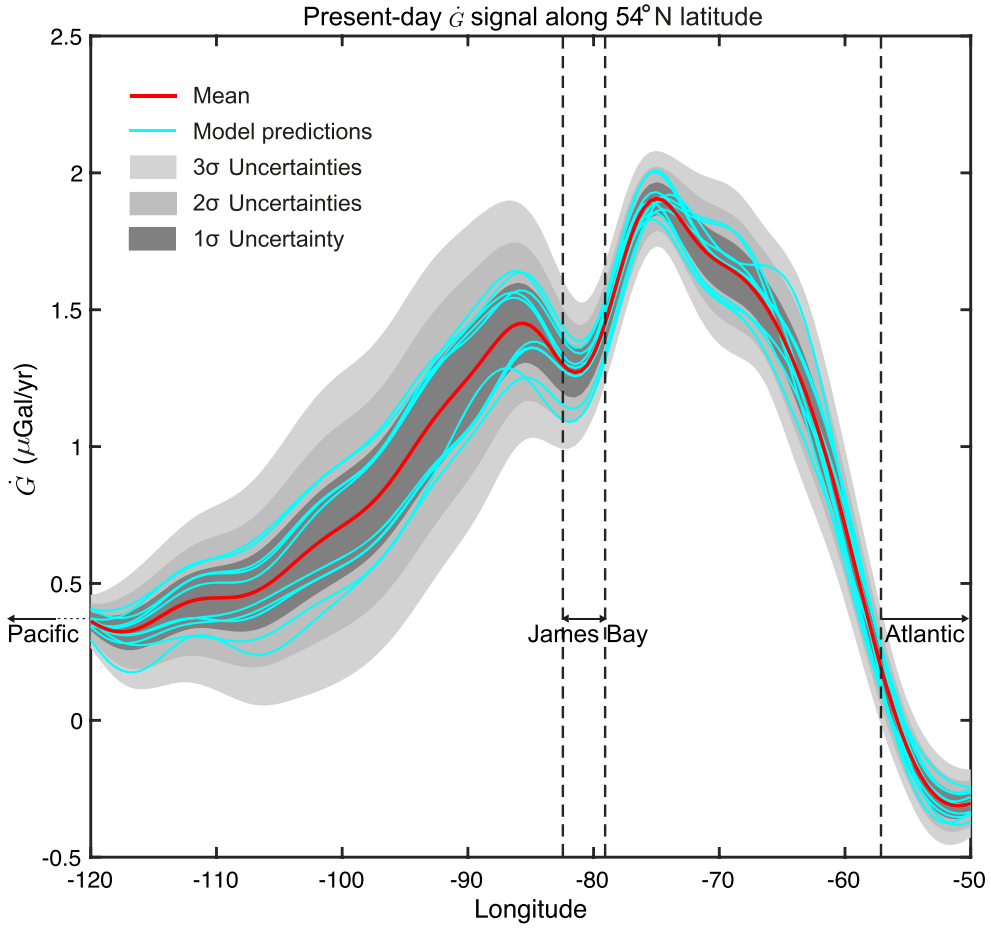

Figure 4. Present-day $\dot{G}$ predictions of the 10 best-fitting models (cyan solid line) and the mean (red solid line) along the 54°N cross section in Figure 3c and 3d. The dark gray-, gray-, and light gray-shaded areas indicate the 1σ, 2σ, and 3σ uncertainties from the mean $\dot{G}$, respectively.

3.2. Present-day $\dot{U}$ and $\dot{G}$ Signals

The mean of the 10 best-fitting GIA models show two maxima of present-day $\dot{U}$ and $\dot{G}$ predictions in western and eastern Hudson Bay with magnitudes over 12 mm/year and 1.8 μGal/year (Figures 3a and 3c). The mean $\dot{U}$ and $\dot{G}$ have a similar distribution pattern, decreasing outwards from the two maxima and close to 0 near the ice margins.

The 2σ uncertainties of $\dot{U}$ and $\dot{G}$ are greatest in southwestern Hudson Bay (>2.4 mm/year and 0.4 μGal/year, Figure 3), which are mainly due to lateral heterogeneity in the lower mantle and consistent with recent sensitivity results of Li et al. (2018). However, the distribution patterns are also affected by the lateral variations of lithospheric thickness, asthenospheric thickness, and viscosity (Figure S12). For example, the 2σ uncertainties centered offshore along the Pacific coast of central North America are mainly due to a low-viscosity asthenosphere in that area (Figure S12). The magnitudes of 2σ uncertainties of $\dot{U}$ and $\dot{G}$ are much smaller, and their patterns are different from the results of Caron et al. (2018) (Figure S13) because they applied a wide range of 1D mantle viscosities and also modified the ice history. As a consequence, not all their model predictions can simultaneously fit deglacial RSL histories and observed present-day $\dot{U}$ and $\dot{G}$ data. If we apply the 20% rule of GRACE (Figure S14), the $\dot{G}$ 2σ uncertainty has a similar magnitude but a different distribution pattern. The 20% rule overestimates the uncertainty in western and eastern Hudson Bay but underestimates the uncertainty near the ice margins, especially in southwestern Hudson Bay where we have the largest $\dot{G}$ uncertainty.

Most of the $\dot{G}$ predictions from the 10 best-fitting models along 54°N latitude fall within 2σ uncertainties from the mean $\dot{G}$ (Figure 4). The largest uncertainties extend from 110°W to 85°W which corresponds to the 2σ uncertainty maximum in southwestern Hudson Bay (Figure 3d). Moving east, the trough in $\dot{G}$ near −80°W is located at James Bay and is followed by increasing $\dot{G}$ that peaks around −75°W. The peak $\dot{G}$ predictions are between ~1.8 and 2.0 μGal/year and correspond with the peak GRACE observations (Peltier et al., 2015). The $\dot{G}$ uncertainties then decrease sharply from 70°W to the Atlantic Ocean.

We compared the mean present-day $\dot{U}$ and $\dot{G}$ predictions including their 2σ uncertainties from the 10 best-fitting models (Figure 3) with observations (Peltier et al., 2015; Sella et al., 2007). 339 out of 348 (97.4%) GNSS site observations from Peltier et al. (2015) are fit by the mean $\dot{U}$ within one observed error bar (Figure 3a). The mean present-day $\dot{G}$ (Figure 3c) prediction accurately fit the double "bulls-eye" structure that evident in GRACE time-dependent gravity observations. Also, the mean present-day $\dot{G}$ prediction fits, both in magnitude and pattern, the GIA-induced $\dot{G}$ signal transformed from GNSS data using the method of Wang et al. (2013) (Figure S4).

4. Conclusions

We provided mean and uncertainties of GIA predictions in North America associated with 3D mantle viscosity profiles (T1A) from an ensemble of 250 Earth models, including 150 3D Earth models that consider lateral variations in mantle viscosity, lithospheric thickness, and sublithospheric and asthenospheric properties. Based on the goodness of fit with the combined RSL data set and the observed present-day $\dot{U}$ and $\dot{G}$ data in North America, we select 10 best-fitting GIA models to compute the mean and 2σ uncertainties of GIA predictions of RSL, $\dot{U}$, and $\dot{G}$. The GIA models show the following:

1. The magnitude of RSL 2σ uncertainties varies across North America with larger uncertainties around Hudson Bay and near previous ice margins of the Laurentide ice sheet along the northern Atlantic and Pacific coasts. The magnitude of uncertainties decreases from the Last Glacial Maximum to present except for the increase in magnitude of the maxima off the west of Hudson Bay and northeastern Pacific coast from 30 to 45 m between 15 and 11 ka BP. The uncertainties patterns do not change temporally until 8 ka BP, after which an area of higher uncertainties emerges in southwestern Hudson Bay that may be entirely due to the uncertainty of the 3D structures.
2. The 2σ uncertainties of the present-day $\dot{U}$ and $\dot{G}$ are centered around the southwestern Hudson Bay with magnitudes around 2.4 mm/year and 0.4 μGal/year, which are different from previous uncertainty study results obtained with 1D Earth model-based analyses.
3. The uncertainties of RSL and present-day $\dot{U}$ and $\dot{G}$ strongly imply that the 3D structures need to be considered in studies of deglacial RSL reconstructions (e.g., Engelhart et al., 2009), future sea-level rise projections (e.g., Love et al., 2016), analysis of vertical land motion from tectonics (e.g., Kreemer et al., 2014; Majewski et al., 2018), and signals of hydrology and ice-mass balance changes from GRACE data (e.g., Shepherd et al., 2018; Wang et al., 2013).

In this study, we have only investigated GIA model prediction uncertainties in North America that is associated with the presence of 3D structure (T1A) but with fixed ICE-6G_C surface loading history. Hence, the uncertainties in surface loading history and correlation between loading history and mantle viscosity are not considered, but there is a need for further investigation (Text S1). In the absence of this analysis, the necessity of including 3D internal viscoelastic structure to provide acceptable fits to observational data remains undetermined. Moreover, an updated RSL data set with more extensive spatial and temporal coverage (e.g., Khan et al., 2019) will be required to further improve constraints on the GIA model. All these caveats suggest the necessity of continuing to update the GIA uncertainty analysis associated with presence of 3D structure as new data become available.

Acknowledgments
We thank Donald Argus and an anonymous reviewer for their very constructive comments, which have helped to improve the manuscript. Patrick Wu received GRF grant 17315316 from the Hong Kong Research Grants Council. Tanghua Li and Benjamin P. Horton are supported by the Singapore Ministry of Education Academic Research Fund MOE2019-T3-1-004 and MOE2018-T2-1-030, the National Research Foundation Singapore, and the Singapore Ministry of Education, under the Research Centers of Excellence initiative. Hansheng Wang is funded by the National Key R & D Program of China (2017YFA0603103) and National Natural Science Foundation of China (41431070 and 41974009). The research of W.R. Peltier at Toronto is supported by NSERC discovery grant A9627. The FE calculation was performed with the ABAQUS package from Hibbitt, Karlsson, and Sorensen Inc. This research is conducted in part using the research computing facilities and/or advisory services offered by Information Technology Services, the University of Hong Kong. This article is a contribution to PALSEA (Palaeo-Constraints on Sea-Level Rise), HOLSEA, and International Geoscience Program (IGCP) Project 639, "Sea-Level Changes from Minutes to Millennia". This work is Earth Observatory of Singapore contribution 293. The mean GIA signals of RSL, U, and G with 1σ, 2σ, and 3σ uncertainties are provided for downloading in DR-NTU (Data) with open access (https://doi.org/10.21979/N9/26AY8H). The deglacial RSL data, observed GNSS data used in this study are from the supplementary information of the corresponding references (with link) that are listed in the References List: Engelhart & Horton, 2012; Engelhart et al., 2015; Hawkes et al., 2016; Khan et al., 2017; Love et al., 2016; Peltier et al., 2015; Vacchi et al., 2018.

References

Argus, D. F., Peltier, W. R., Drummond, R., & Moore, A. W. (2014). The Antarctica component of postglacial rebound model ICE-6G_C (VM5a) based on GPS positioning, exposure age dating of ice thicknesses, and relative sea level histories. *Geophysical Journal International*, *198*(1), 537–563.

Austermann, J., Mitrovica, J. X., Latychev, K., & Milne, G. A. (2013). Barbados-based estimate of ice volume at Last Glacial Maximum affected by subducted plate. *Nature Geoscience*, *6*(7), 553–557.
Barnhardt, W. A., Gehrels, W. R., & Kelley, J. T. (1995). Late Quaternary relative sea-level change in the western Gulf of Maine: Evidence for a migrating glacial forebulge. *Geology*, *23*(4), 317–320.
Bunge, H.-P., & Grand, S. P. (2000). Mesozoic plate-motion history below the northeast Pacific Ocean from seismic images of the subducted Farallon slab. *Nature*, *405*(6784), 337–340. https://doi.org/10.1038/35012586
Caron, L., Ivins, E. R., Larour, E., Adhikari, S., Nilsson, J., & Blewitt, G. (2018). GIA model statistics for GRACE hydrology, cryosphere, and ocean science. *Geophysical Research Letters*, *45*(5), 2203–2212. https://doi.org/10.1002/2017GL076644
Clark, J., Mitrovica, J. X., & Latychev, K. (2019). Glacial isostatic adjustment in Central Cascadia: Insights from three-dimensional Earth modeling. *Geology*, *47*(4), 295–298.
Clark, J. A., Farrell, W. E., & Peltier, W. R. (1978). Global changes in postglacial sea level: A numerical calculation 1. *Quaternary Research*, *9*(3), 265–287.
Ekström, G., & Dziewonski, A. M. (1998). The unique anisotropy of the Pacific upper mantle. *Nature*, *394*(6689), 168–172.
Engelhart, S. E., & Horton, B. P. (2012). Holocene sea level database for the Atlantic coast of the United States. *Quaternary Science Reviews*, *54*, 12–25. https://doi.org/10.1016/j.quascirev.2011.09.013
Engelhart, S. E., Horton, B. P., Douglas, B. C., Peltier, W. R., & Törnqvist, T. E. (2009). Spatial variability of late Holocene and 20th century sea-level rise along the Atlantic coast of the United States. *Geology*, *37*(12), 1115–1118.
Engelhart, S. E., Vacchi, M., Horton, B. P., Nelson, A. R., & Kopp, R. E. (2015). A sea-level database for the Pacific coast of Central North America. *Quaternary Science Reviews*, *113*, 78–92. https://doi.org/10.1016/j.quascirev.2014.12.001
Fairbanks, R. G. (1989). A 17,000-year glacio-eustatic sea level record: Influence of glacial melting rates on the Younger Dryas event and deep-ocean circulation. *Nature*, *342*(6250), 637–642.
Hawkes, A. D., Kemp, A. C., Donnelly, J. P., Horton, B. P., Peltier, W. R., Cahill, N., et al. (2016). Relative sea-level change in northeastern Florida (USA) during the last~ 8.0 ka. *Quaternary Science Reviews*, *142*, 90–101. https://doi.org/10.1016/j.quascirev.2016.04.016
Hill, E. M., Davis, J. L., Tamisiea, M. E., & Lidberg, M. (2010). Combination of geodetic observations and models for glacial isostatic adjustment fields in Fennoscandia. *Journal of Geophysical Research: Solid Earth*, *115*(B7).
Karato, S. I. (2008). *Deformation of Earth materials: An introduction to the rheology of Earth materials*. Press, ISBN: Cambridge Univ.
Karegar, M. A., Dixon, T. H., Malservisi, R., Kusche, J., & Engelhart, S. E. (2017). Nuisance flooding and relative sea-level rise: The importance of present-day land motion. *Scientific Reports*, *7*(1), 11,197.
Kennett, B. L. N., & TkalČić, H. (2008). Dynamic Earth: Crustal and mantle heterogeneity. *Australian Journal of Earth Sciences*, *55*(3), 265–279.
Khan, N. S., Ashe, E., Horton, B. P., Dutton, A., Kopp, R. E., Brocard, G., et al. (2017). Drivers of Holocene sea-level change in the Caribbean. *Quaternary Science Reviews*, *155*, 13–36. https://doi.org/10.1016/j.quascirev.2016.08.032
Khan, N. S., Horton, B. P., Engelhart, S., Rovere, A., Vacchi, M., Ashe, E. L., et al. (2019). Inception of a global atlas of sea levels since the Last Glacial Maximum. *Quaternary Science Reviews*, *220*, 359–371.
Kreemer, C., Blewitt, G., & Klein, E. C. (2014). A geodetic plate motion and global strain rate model. *Geochemistry, Geophysics, Geosystems*, *15*(10), 3849–3889.
Kuchar, J., Milne, G., & Latychev, K. (2019). The importance of lateral Earth structure for North American glacial isostatic adjustment. *Earth and Planetary Science Letters*, *512*, 236–245.
Lau, H. C. P., Austermann, J., Mitrovica, J. X., Crawford, O., Al-Attar, D., & Latychev, K. (2018). Inferences of mantle viscosity based on ice age data sets: The bias in radial viscosity profiles due to the neglect of laterally heterogeneous viscosity structure. *Journal of Geophysical Research: Solid Earth*, *123*(9), 7237–7252.
Li, T., & Wu, P. (2018). Laterally heterogeneous lithosphere, asthenosphere and sub-lithospheric properties under Laurentia and Fennoscandia from glacial isostatic adjustment. *Geophysical Journal International*, *216*(3), 1633–1647.
Li, T., Wu, P., Steffen, H., & Wang, H. (2018). In search of laterally heterogeneous viscosity models of glacial isostatic adjustment with the ICE-6G_C global ice history model. *Geophysical Journal International*, *214*(2), 1191–1205.
Love, R., Milne, G. A., Tarasov, L., Engelhart, S. E., Hijma, M. P., Latychev, K., et al. (2016). The contribution of glacial isostatic adjustment to projections of sea-level change along the Atlantic and gulf coasts of North America. *Earth's Future*, *4*(10), 440–464. https://doi.org/10.1002/2016EF000363
Majewski, J. M., Switzer, A. D., Meltzner, A. J., Parham, P. R., Horton, B. P., Bradley, S. L., et al. (2018). Holocene relative sea-level records from coral microatolls in Western Borneo, South China Sea. *The Holocene*, *28*(9), 1431–1442.
Melini, D., & Spada, G. (2019). Some remarks on glacial isostatic adjustment modelling uncertainties. *Geophysical Journal International*, *218*(1), 401–413.
Nield, G. A., Whitehouse, P. L., van der Wal, W., Blank, B., O'Donnell, J. P., & Stuart, G. W. (2018). The impact of lateral variations in lithospheric thickness on glacial isostatic adjustment in West Antarctica. *Geophysical Journal International*, *214*(2), 811–824.
Peltier, W. R. (2005). On the hemispheric origins of meltwater pulse 1a. *Quaternary Science Reviews*, *24*(14–15), 1655–1671.
Peltier, W. R., Argus, D. F., & Drummond, R. (2015). Space geodesy constrains ice age terminal deglaciation: The global ICE-6G_C (VM5a) model. *Journal of Geophysical Research: Solid Earth*, *120*(1), 450–487.
Riva, R. E. M., Gunter, B. C., Urban, T. J., Vermeersen, B. L. A., Lindenbergh, R. C., Helsen, M. M., et al. (2009). Glacial isostatic adjustment over Antarctica from combined ICESat and GRACE satellite data. *Earth and Planetary Science Letters*, *288*(3–4), 516–523.
Roy, K., & Peltier, W. R. (2015). Glacial isostatic adjustment, relative sea level history and mantle viscosity: Reconciling relative sea level model predictions for the US east coast with geological constraints. *Geophysical Journal International*, *201*(2), 1156–1181.
Schumacher, M., King, M. A., Rougier, J., Sha, Z., Khan, S. A., & Bamber, J. L. (2018). A new global GPS data set for testing and improving modelled GIA uplift rates. *Geophysical Journal International*, *214*(3), 2164–2176.
Sella, G. F., Stein, S., Dixon, T. H., Craymer, M., James, T. S., Mazzotti, S., & Dokka, R. K. (2007). Observation of glacial isostatic adjustment in "stable" North America with GPS. *Geophysical Research Letters*, *34*(2). https://doi.org/10.1029/2006GL027081
Shennan, I., & Horton, B. (2002). Holocene land-and sea-level changes in Great Britain. *Journal of Quaternary Science: Published for the Quaternary Research Association*, *17*(5–6), 511–526.
Shepherd, A., Ivins, E., Rignot, E., Smith, B., Van Den Broeke, M., Velicogna, I., et al. (2018). Mass balance of the Antarctic ice sheet from 1992 to 2017. *Nature*, *558*, 219–222.
Simon, K. M., Riva, R. E. M., Kleinherenbrink, M., & Tangdamrongsub, N. (2017). A data-driven model for constraint of present-day glacial isostatic adjustment in North America. *Earth and Planetary Science Letters*, *474*, 322–333.

Slangen, A. B. A., Katsman, C. A., de Wal, R. S. W., Vermeersen, L. L. A., & Riva, R. E. M. (2012). Towards regional projections of twenty-first century sea-level change based on IPCC SRES scenarios. *Climate Dynamics*, *38*(5–6), 1191–1209.

Spada, G., Antonioli, A., Cianetti, S., & Giunchi, C. (2006). Glacial isostatic adjustment and relative sea-level changes: the role of lithospheric and upper mantle heterogeneities in a 3-D spherical Earth. *Geophysical Journal International*, *165*(2), 692–702.

Stea, R. R., Fader, G. B. J., Scott, D. B., & Wu, P. (2001). Glaciation and relative sea-level change in Maritime Canada. *Special Papers-Geological Society of America*, 35–50.

Tushingham, A., & Peltier, W. R. (1991). Ice-3G: A new global model of late Pleistocene deglaciation based upon geophysical predictions of post-glacial relative sea level change. *Journal of Geophysical Research: Solid Earth*, *96*(B3), 4497–4523.

Vacchi, M., Engelhart, S. E., Nikitina, D., Ashe, E. L., Peltier, W. R., Roy, K., et al. (2018). Postglacial relative sea-level histories along the eastern Canadian coastline. *Quaternary Science Reviews*, *201*, 124–146. https://doi.org/10.1016/j.quascirev.2018.09.043

Wang, H., Jia, L., Steffen, H., Wu, P., Jiang, L., Hsu, H., et al. (2013). Increased water storage in North America and Scandinavia from GRACE gravity data. *Nature Geoscience*, *6*(1), 38–42.

Wang, H., & Wu, P. (2006). Effects of lateral variations in lithospheric thickness and mantle viscosity on glacially induced surface motion on a spherical, self-gravitating Maxwell Earth. *Earth and Planetary Science Letters*, *244*(3), 576–589.

Wu, P. (2004). Using commercial finite element packages for the study of earth deformations, sea levels and the state of stress. *Geophysical Journal International*, *158*(2), 401–408.

Wu, P., Steffen, H., & Wang, H. (2010). Optimal locations for GPS measurements in North America and northern Europe for constraining glacial isostatic adjustment. *Geophysical Journal International*, *181*(2), 653–664.

Wu, P., Wang, H., & Steffen, H. (2013). The role of thermal effect on mantle seismic anomalies under Laurentia and Fennoscandia from observations of glacial isostatic adjustment. *Geophysical Journal International*, *192*(1), 7–17.

Yousefi, M., Milne, G. A., Love, R., & Tarasov, L. (2018). Glacial isostatic adjustment along the Pacific coast of Central North America. *Quaternary Science Reviews*, *193*, 288–311.